



Investigation of air temperature on the nightside of Venus derived from VIRTIS-H on board Venus-Express

A. Migliorini ^{a,*}, D. Grassi ^b, L. Montabone ^{c,d}, S. Lebonnois ^c, P. Drossart ^e, G. Piccioni ^a

^a IASF-INAF, via del Fosso del Cavaliere, 100, 00133 Rome, Italy

^b IFSI-INAF, via del Fosso del Cavaliere, 100, 00133 Rome, Italy

^c Laboratoire de Meteorologie Dynamique, Jussieu, Box 99, 75252 Paris, France

^d AOPP, Dept. of Physics, University of Oxford, Parks Road, Oxford OX14 PU, UK

^e LESIA, 5, Place Jules Janssen, 92195 Meudon, Paris, France

ARTICLE INFO

Article history:

Available online 4 August 2011

Keywords:

Venus
Atmospheres, Structure
Atmospheres, Dynamics
Radiative transfer

ABSTRACT

We present the spatial distribution of air temperature on Venus' night side, as observed by the high spectral resolution channel of VIRTIS (Visible and Infrared Thermal Imaging Spectrometer), or VIRTIS-H, on board the ESA mission Venus Express. The present work extends the investigation of the average thermal fields in the northern hemisphere of Venus, by including the VIRTIS-H data. We show results in the pressure range of 100–4 mbar, which corresponds to the altitude range of 65–80 km. With these new retrievals, we are able to compare the thermal structure of the Venus' mesosphere in both hemispheres.

The major thermal features reported in previous investigations, i.e. the cold collar at about 65–70° latitude, 100 mbar pressure level, and the asymmetry between the evening and morning sides, are confirmed here. By comparing the temperatures retrieved by the VIRTIS spectrometer in the North and South we find that similarities exist between the two hemispheres. Solar thermal tides are clearly visible in the average temperature fields. To interpret the thermal tide signals (otherwise impossible without day site observations), we apply model simulations using the Venus global circulation model Venus GCM (Lebonnois, S., Hourdin, F., Forget, F., Eymet, V., Fournier, R. [2010b]. International Venus Conference, Aussois, 20–26 June 2010) of the Laboratoire de Météorologie Dynamique (LMD). We suggest that the signal detected at about 60–70° latitude and pressure of 100 mbar is a diurnal component, while those located at equatorial latitudes are semi-diurnal. Other tide-related features are clearly identified in the upper levels of the atmosphere.

© 2011 Elsevier Inc. All rights reserved.

1. Introduction

Venus has been investigated since the early 1960s, by several US and Russian missions. The extended chronology of these missions is presented in Moroz et al. (2002) and Titov et al. (2002).

The US Mariner series carried out several planetary flybys, providing important information about Venus' atmosphere. In addition, the Soviet Venera 4–8 and 11–14 missions, which delivered entry probes, and the Venera 9 and 10, which both combined an orbiter and a probe, allowed an in depth study of the venusian atmosphere from space and in situ.

In 1983–84 the Venera 15 and 16 orbiters investigated the atmosphere of the planet in the thermal infrared with the Fourier

spectrometer aboard (Oertel et al., 1985a,b; Moroz et al., 1986), retrieving the thermal structure from the 15 μm CO₂ band.

In the 1980s and 1990s, investigations of Venus were carried out by: the Vega 1 and 2 balloons (Linkin et al., 1986, 1987; Crisp et al., 1990), the flyby performed by the Galileo mission in 1990 on its route to Jupiter, and the two flybys by the Cassini–Huygens spacecraft on 1997 and 1999 (Baines et al., 2000).

Several ground-based observations added information about the atmosphere below the clouds (Bezard et al., 1990; Pollack et al., 1993; Meadow and Crisp, 1996; Taylor et al., 1997).

Temperatures in the Venus atmosphere have been investigated in detail by entry probes that returned accurate profiles at very high vertical resolution and in a wide range of altitudes (cf. Seiff, 1983, for an extensive review). Up to about 40 km, the temperature profile is considered to be quite similar over the entire planet because the latitude and day–night variations are less than 5 K. On the other hand, in the altitude range 60–100 km, inside and above the cloud layer, variability with latitude and local time was significant, though deeper studies are required to better understand and quantify this variability.

* Corresponding author. Fax: +39 0645488188.

E-mail addresses: Alessandra.Migliorini@iasf-roma.inaf.it (A. Migliorini), [Davide.Grassi@ifsi-roma.inaf.it](mailto: Davide.Grassi@ifsi-roma.inaf.it) (D. Grassi), [montabone@atm.ox.ac.uk](mailto: montabone@atm.ox.ac.uk) (L. Montabone), [Sebastien.Lebonnois@lmd.jussieu.fr](mailto: Sebastien.Lebonnois@lmd.jussieu.fr) (S. Lebonnois), [pierre.drossart@obspm.fr](mailto: pierre.drossart@obspm.fr) (P. Drossart), [Giuseppe.Piccioni@iasf-roma.inaf.it](mailto: Giuseppe.Piccioni@iasf-roma.inaf.it) (G. Piccioni).

The thermal structure of Venus below 60 km was investigated using data from Venera 10–12 probes and the Pioneer Venus probes, which resulted in the creation of the Venus International Reference Atmosphere (VIRA) models, currently used by the scientific community for Venus atmosphere modelling (Seiff et al., 1985). VIRA allows modelling the middle atmospheric temperature profiles in five latitudinal ranges, 30°, 45°, 60°, 75° and 85°. The accuracy of the profiles is limited because not representative of the whole atmosphere.

The mesosphere in the altitude range 60–100 km was investigated by the VEGA 2 probe. The thermal structure was probed in the northern hemisphere, and discussed in Zasova et al. (2007).

The European mission to Venus, Venus Express, was launched in November 2005 and has been in orbit around the planet since April 2006. This mission extensively explores Venus on a long time scale. Because of the spacecraft's eccentric polar orbit (its altitude above the planet is 250 and 66,000 km at pericentre and apocentre, respectively), the southern hemisphere is optimally viewed at nadir especially by VIRTIS-M, the mapping channel, (for results see Grassi et al., 2010). In addition, after more than 4 years in orbit, the high resolution channel of VIRTIS, named VIRTIS-H, has provided good coverage of both the northern and southern hemispheres. However, the data are limited to the night side due to the current retrieval method.

In the present paper, we describe the average temperature retrievals obtained by the VIRTIS-H observational data, which cover the period from the orbit insertion (April 2006) to January 2010. We briefly review the retrieval technique, already successfully applied to the data acquired by VIRTIS-M (Grassi et al., 2008, 2010), and then report the results in Section 3. A discussion about dynamical implications is included in Section 4.

2. Observations with VIRTIS-H on Venus Express

The Visible and Infrared Thermal Imaging Spectrometer (VIRTIS) is one of the experiments included in the scientific payload of ESA's Venus Express mission (Titov et al., 2006). The instrument consists of two optical subsystems: VIRTIS-M and VIRTIS-H. VIRTIS-M is an imaging spectrometer in the range from 0.3 to 5.1 μm divided in two channels, VIS and IR, covering the range 0.3–1.1 and 1.0–5.1 μm with a spectral sampling of about 2 and 10 nm respectively. VIRTIS-H, a point spectrometer with a relatively higher spectral resolution but no imaging capability, operates in the range from 2 to 5 μm , with a typical spectral sampling of 1.5 nm, variable along the range at the selected spectral order. The VIRTIS-M and -H instantaneous field-of-view (IFOV) is 0.25×0.25 mrad (for an individual pixel) and 1.74×0.58 mrad, respectively. These figures, applied to the Venus Express orbital parameters, lead to projected horizontal resolution for individual pixels of 16.5×16.5 km and 115×38 km for -M and -H respectively, in the apocenter case. A complete description of the instrument and its performances is given by Piccioni et al. (in press).

For this study, the zeroth order of VIRTIS-H was used, which covers the spectral range 4.0–4.97 μm , with a spectral resolution of 2.5 nm at 4.3 μm . The spectra are then sampled in 432 discrete wavelengths for each dispersion order, although the first tens of pixels on the right side (short wavelengths) of the focal plane array usually yield smaller radiances than expected because of the low grating efficiency on the edges of the orders, thus reducing their effective spectral ranges. Another peculiarity of the array reading system that we had to take into account in our processing methods is the difference in fluxes between odd and even pixels along a given spectrum. Nevertheless, this peculiarity is partially corrected by the calibration process, yielding a few percent difference in the absolute intensities between even and odd pixels.

The retrieval method described in the following subsection has been applied to all the VIRTIS-H data suitable for this study, acquired up to January 2010 (that is, up to Venus Express orbit number 1379). About 3×10^4 spectra have been collected and averaged, in order to obtain the mean temperature maps.

2.1. Retrieval method

Infrared observations take advantage of the variability of CO_2 opacity with wavelength in order to retrieve, by inversion, the temperature profile from the gas thermal emission. Since the technique exploits the ubiquitous atmospheric emission, large regions can be readily mapped. Consequently, infrared spectroscopy, despite a vertical resolution and a retrieval error worse than other remote sensing techniques, has a relevant statistical value to build spatially-extensive datasets. Even with a complete knowledge of the vertical distributions of aerosols and gases, air temperatures and optical properties of suspended materials, the analytical determination of the expected radiation field is not usually possible; consequently, it has to be estimated numerically.

The inversion code to retrieve temperature is based on the radiative transfer equation, as described in Grassi et al. (2008). It is computed for 67 pressure levels, covering the range 1200–0.005 mbar, which approximately corresponds to the altitude range from about 50 to about 105 km. Once the pressure level is fixed, the night side spectrum of Venus is simulated, starting from an appropriate initial vertical profile selected from those available in the VIRA, in order to guess the initial temperature. A relaxation method is used to iteratively compare each simulated spectrum with the observed one, in order to refine the simulation and find out the best parameters to fit the observations. A χ^2 test, obtained by comparing the spectral region around 4.3 μm on the two spectra, quantifies the goodness of the fit. To increase the signal to noise ratio (SNR), spectra were averaged in groups of 10, providing that distance between single spectra does not exceed 2° , sun-zenith angle greater than 95° and emergence angle smaller than 30° . Temperature error bars are within 4 K in the pressure range 100–4 mbar, which covers the altitude range from 65 to 80 km; hence the investigation is limited to this region.

2.2. Filtering process

Prior to further processing, we removed from our dataset individual retrievals derived from observations acquired either at emission angles greater than 30° or at sun-zenith angles lower than 95° . The former filter was applied to reduce the weight of temperature profiles affected by larger modelling uncertainty. The latter filter allows to remove completely the effects of the scattering of solar photons. This radiation source has a non negligible effect on radiances measured at the centre of the 4.3 μm band even when the Sun is few degrees below the horizon and adversely affects temperatures retrieved above 80 km. The two filters allowed more than 3×10^4 profiles to be available for further analysis. The coverage of the usable data is shown in Fig. 1.

We classified individual temperature profiles on the basis of latitude and subsolar longitude at the time of acquisition (the latter quantity being equivalent to local time), and binned in $5^\circ \times 5^\circ$ (latitude–longitude) wide bins.

For each given pressure level of the reference retrieval grid, the N individual profiles in the bin provided N independent estimates. Mean temperature T_0 and standard deviation σ were then computed for each bin. Data beyond 2σ were rejected, and new mean and standard deviation values were calculated in each bin. Finally, we obtained three-dimensional matrices of air mean temperatures and standard deviations as a function of latitude, local time and pressure. The limit of 2σ was required to filter out the retrieval

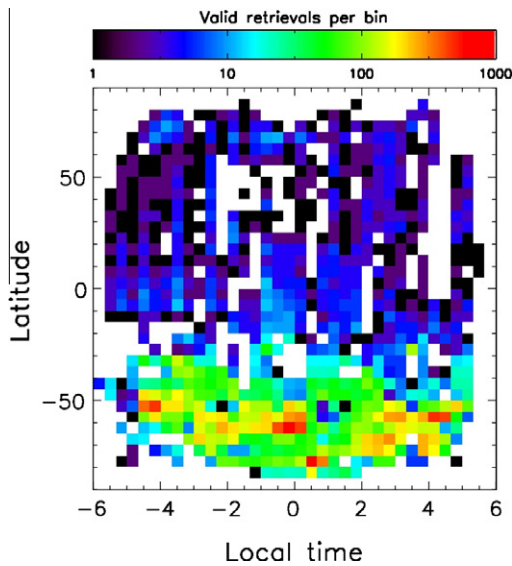


Fig. 1. Map of the available VIRTIS-H data, distributed in the latitude–local time plane. In the southern hemisphere, a better coverage is manifest. A total of 3×10^4 spectra were used in this study.

results mostly affected by the numerical instability in the relaxation inverse techniques, as described in Grassi et al. (2008). Nevertheless, it was verified that the application of the 2σ limit does not change the general trend of the temperature maps.

Unstable retrievals are not associated with specific conditions or specific regions of Venus atmosphere. They are mostly related to residual calibration issues in the input data. These issues can occur more frequently in specific parts of VIRTIS focal plane (some clusters of pixels may show systematic shifts in the signal level) or can be randomly distributed (due to cosmic rays on the detector or spikes in the electronics) and eventually result in Venus spectra without a physical meaning.

The proper interpretation of the fields considered here accounts for the different statistical weights of regions in the latitude–local time space.

The averaging process is extended over the entire analyzed population acquired at a fixed local time. This implies an assumption on the minor role played by possible seasonal trends in determining the atmospheric thermal structure. Even if this behaviour is expected on the basis of the low values of Venus' orbital eccentricity and polar axis inclination, we performed nonetheless a quantitative analysis. This investigation confirmed that – for a given pressure level – data inside each bin do not present any systematic correlation with the Julian Date of acquisition beyond the confidence levels set by random retrieval error and data dispersion.

It shall be noted that the overall VIRTIS-H data processing contained two consecutive averaging processes. The first one involved the radiances, binned on the image plane. Resulting average radiances were used as input for temperature retrieval code. The second one involved the output temperatures, binned in latitude–local time bins from which the temperature is retrieved. This scheme has a twofold advantage with respect to averaging all radiances in latitude–local time bins and then performs the temperature retrieval. Firstly, each average radiance derives from the same number of input spectra, implying the same effective radiometric error and the same retrieval error for each derived temperature profile. Secondly, the scheme allowed different sizes of latitude–local time bins to be tested and allowed possible seasonal effects to be studied without having to repeat the time-consuming temperature retrieval.

Tests on different bin sizes for the second average demonstrated that the results presented in this paper remain quantitatively the

same. Namely, we verified the invariance of the results with the bin size for different possible sections of the three-dimensional matrices of air mean temperatures and standard deviations: latitude/local time, latitude/pressure, local time/pressure.

3. Results

The VIRTIS-H channel provided an overall picture of the temperature fields on both the northern and southern hemispheres, although data are quite sparse in the northern hemisphere (Fig. 1).

In the following, we discuss results of air temperature average maps at selected pressure levels. Variability with local time and latitude are taken into account.

At 100 mbar (Fig. 2a), which approximately corresponds to the cloud top altitude at a height of 65 km, temperatures are higher on the dusk side with respect to the dawn side, but with a local maximum at equatorial latitudes between 22 h and 24 h Local Time (LT). In this map at about midnight, an increase of about 10 K is observed near the equator compared to the mid-latitudes. This temperature increase at the anti-solar point is observed for the first time in these data, although it was indicated in the previous study with VIRTIS-M data in the southern hemisphere (Grassi et al., 2010). The cold collar structure, observed for the first time by Taylor et al. (1980) on Pioneer Venus Orbiter data and located at about 60° latitude in both hemispheres, is colder and more prominent on the dawn side. The temperatures show the coldest region at about 3 h in both hemispheres, although we cannot rule out a further decrease toward the terminator, where data are lacking. In the southern hemisphere, however, the above mentioned cold temperature region corresponds to the minimum clearly observed in VIRTIS-M data (see Fig. 3a in Grassi et al. (2010)), where the better coverage of the region makes it more certain.

Moving to higher altitudes (about 70 km, or 31.6 mbar, see Fig. 2b), the cold collar structure disappears while the temperature increases toward the pole in both hemispheres. A variation of about 10 K is observed from equatorial to polar latitudes. Additionally, the temperature field is slightly warmer from 20 h to 21 h at almost all the latitudes. Though this map seems to confirm the findings previously obtained with the M-channel of VIRTIS, the air temperature at 31.6 mbar is about 5 K colder on average in the map shown in Fig. 2b than in the corresponding case in Grassi et al. (2010). As seen in the map in Fig. 2b, the dawn side is colder than the dusk side which agrees with the M-channel analysis. This difference may be caused by a different effective vertical sampling in the retrieval due to the different spectral resolution of -H and -M.

At the pressure level of 12.6 mbar (a height of about 75 km, Fig. 2c), a local minimum in temperature is observed at mid latitudes close to midnight, and local maxima are observed at 20–21 h and 23 h LT in both hemispheres. At low latitudes close to equator, the minimum appears displaced more toward the morning side. The temperature is about 5–10 K warmer at polar than mid latitudes.

At 4 mbar (about 80 km) temperature is on average 10 K lower than at 12.6 mbar, as shown in Fig. 2d. The dawn side is the warmest over the entire considered local time. A local temperature minimum (T about 200 K) is observed at mid latitudes between 20–22 h LT in the southern hemisphere and perhaps a weaker one at mid latitudes at 22 h LT in the northern hemisphere. Another possible minimum appears located at lower latitudes in the 5 h LT region, in contrast to the surrounding area.

We now consider cross-sections of the thermal fields at selected latitudes.

At 77.5°S (Fig. 3a), the air temperature is locally colder in the cold collar region (about 100 mbar) on the morning side, while it

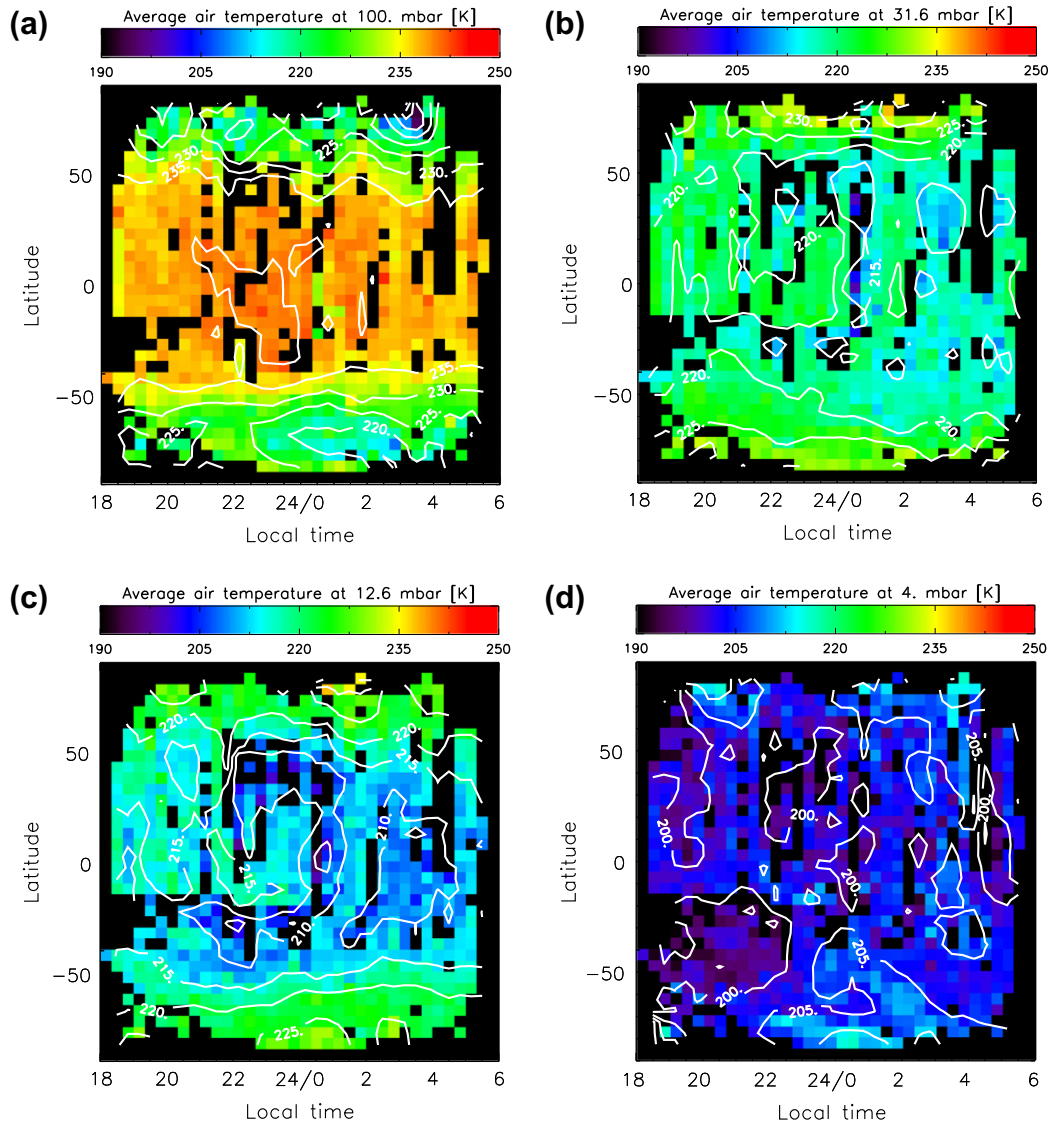


Fig. 2. Air temperature maps at 100 mbar (a, about 65 km), 31.6 mbar (b, about 70 km), 12.6 mbar (c, about 75 km) and 4 mbar (d, about 80 km).

is warmer at 3 h LT moving to 10 mbar. On average, the temperature decreases with decreasing pressure levels. Some wave-like structures could possibly be present at about 5 mbar, in the dawn quadrant, based on the temperature fields. A similar trend is recorded in the northern hemisphere (Fig. 3b), despite the sparser sampling in this region. Moreover, the northern hemisphere seems to be a little bit warmer than the southern, in the pressure range 100–10 mbar, from midnight to 2 h. In general, the high latitude maps show the highest contrast in temperature, behaviour which is very likely correlated with the polar vortex dynamics.

At about 57° (Fig. 3c and d), air temperature fields become more uniform over time. However, a local maximum is possibly detected at 2 h LT, below the 10 mbar level (upper part of the plot). In the cold collar region, the local time of early morning presents a local temperature minimum at the lowest altitudes (about 100 mbar in pressure). No substantial differences between the two hemispheres are observed (Fig. 3c and d).

At intermediate latitudes (37.5°S and N, Fig. 3e and f), the region close to the top of the cloud deck (about 100 mbar, which corresponds approximately to 65 km) becomes warmer, with air temperature decreasing with pressure. The region below 10 mbar

(above 75 km) is characterized by a local maximum close to midnight, on both hemispheres. In the same region, morning side appears as the warmest in both hemispheres.

Close to the equator (Fig. 3g), temperature of cloud top slightly decreases towards both terminators. Local maxima and minima of temperature are present in the pressure region 10–1 mbar.

The temperature structure does not appear to be symmetric with respect to local time. As already stated, the cold collar structure is more pronounced in the morning side, as well as the polar warming. In addition, above 10 mbar, air temperature in the equatorial region is slightly colder during late evening than at morning.

The VIRTIS-H data confirm overall the previous findings for the southern hemisphere, obtained by using the VIRTIS-M data as discussed in Grassi et al. (2008, 2010), and further extend the results to the northern hemisphere.

The great variety of features observed and described above could be considered as evidence of dynamics in Venus' atmosphere at 65–80 km height. Maxima and minima in temperature, observed in the southern and northern hemispheres at 100 mbar, could be interpreted as sun-synchronous waves, with a wavelength of about 180° longitude and a phase that shifts moving towards the equator.

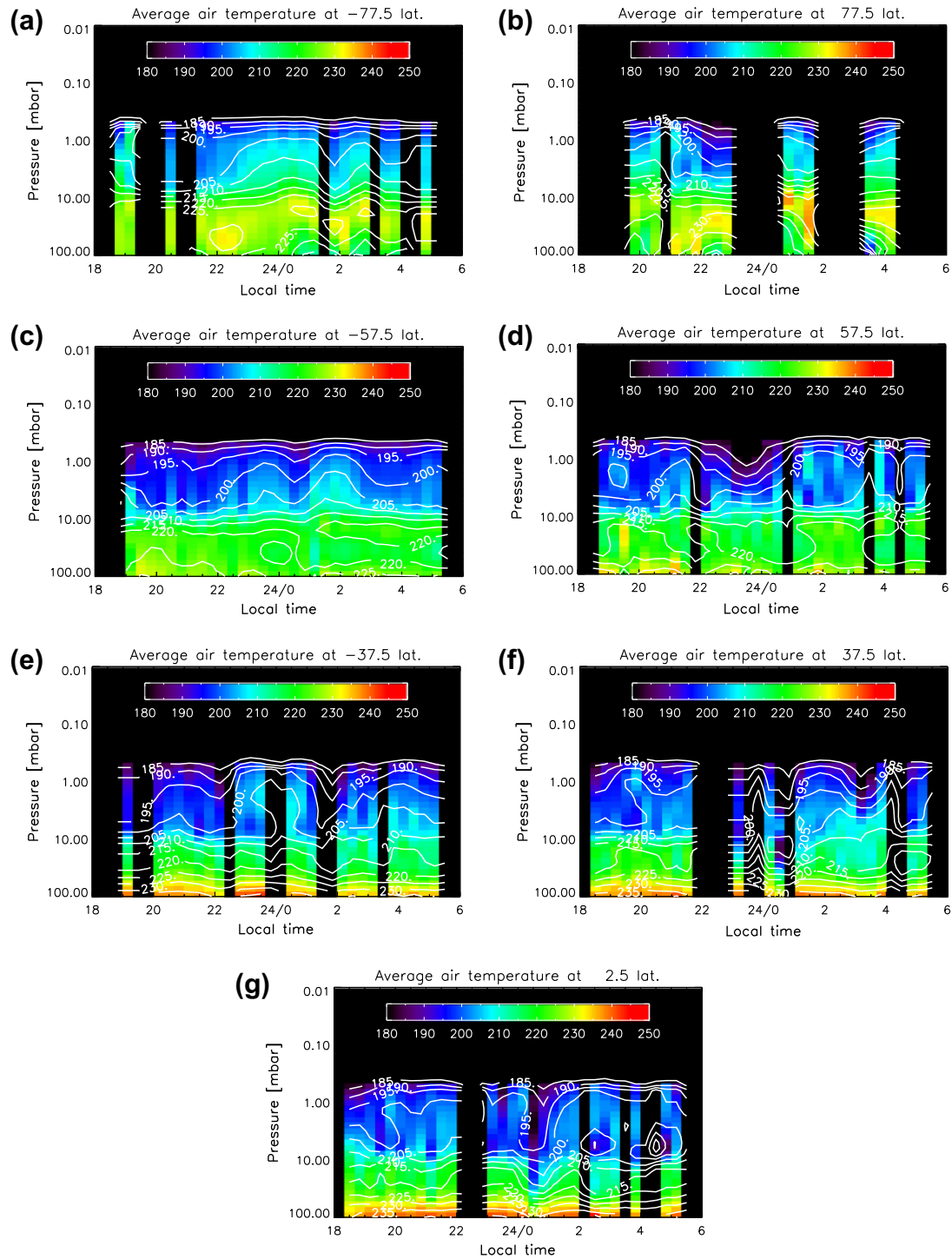


Fig. 3. Temperature maps at selected latitudes: at 77.5°S (a), 77.5°N (b), 57.5°S (c), 57.5°N (d), 37.5°S (e), 37.5°N (f) and 2.5°N (g). Horizontal axis represents local time (in h) while the vertical one is pressure (in mbar). The northern and the southern hemispheres are compared in this case. There are clear similarities in the thermal fields. Moreover, no significant variations in the temperature range are observed from one hemisphere to the other.

4. Discussion

A satisfactory agreement between average temperature retrieved from VIRTIS-H and Orbiter Infrared Radiometer (OIR) of the Pioneer Venus mission (Schofield and Taylor, 1983) was found at equatorial latitudes (see Fig. 4). In Fig. 4, the thermal isolines derived from the OIR PV data are superimposed to the map at 7.5°S in the longitude–pressure plane. A better agreement is observed in the pressure range 100–10 mbar, while a significant overestima-

tion by about 15–20 K is recorded in the case of our retrieval method with respect to OIR data at pressure levels lower than 10 mbar. The good agreement, at least for the mid-high pressure part, is obtained despite the differences in the spectral range and in the width of the weighting functions used for the retrievals. Long-term variability may be one candidate, since the PV and Venus Express missions differ by about 30 years in time. OIR data were acquired during a maximum of the solar cycle, while VIRTIS data refer to a minimum. EUV (Extreme Ultraviolet) heating varies with the solar

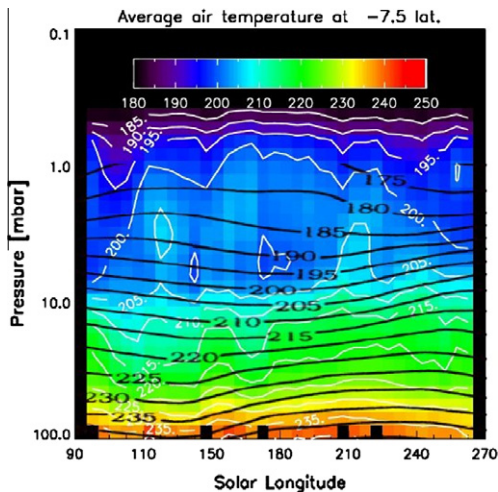


Fig. 4. Comparison between the retrieved temperature with VIRTIS and the OIR PV instrument. The black curves represent the OIR temperature levels, superimposed on the thermal field retrieved from VIRTIS data, at 7.5°S.

cycles, and could have some impact in the circulation pattern that occurs in the region covered by VIRTIS observations, though it might not satisfactorily explain the discrepancy between OIR and VIRTIS data.

The variety of features described in Section 3 confirms the tight connection between dynamics and thermal fields in Venus' atmosphere between 65 and 90 km. A Hadley cell that extends throughout the entire northern (or southern) hemisphere has long been postulated as the main cause of the temperature increase from mid-latitudes to the pole (Taylor et al., 1980). This polar warming would occur by adiabatic compression of air in the descending branch of the Hadley cell at polar latitudes.

Patterns of temperature versus local time at 100 mbar (Fig. 2a) are of particular interest. Thermal tides in Venus' mesosphere have been recognized in their wavenumber-1 and/or wavenumber-2 components in OIR (Schofield and Taylor, 1983), FTS (Zasova et al., 2007) and VeRa (Tellmann et al., 2009) data, mainly in the northern hemisphere. The observations by VIRTIS are consistent with the effects of sun-synchronous waves, which can be components of the thermal tide, particularly strong in the region of the southern cold collar (100 mbar, 65°) and at equatorial latitudes. Only night side retrievals by VIRTIS are available at the moment, therefore a full characterization of such waves in term of wavenumbers and phases cannot be provided in this paper. Nevertheless, we can suggest a possible interpretation, based on results from a global circulation numerical model.

The relative amplitudes of the different components of the thermal tides and other significant atmospheric waves have been recently investigated by Lebonnois et al. (2010a) using Venus atmospheric global circulation models (GCMs). The LMD Venus GCM model (Lebonnois et al., 2010a) was applied to interpret our observations. Numerical simulations were performed starting from initial conditions describing an atmosphere already in superrotation (Lebonnois et al., 2010b). The zonal wind field thus obtained is characterized by zonal winds between surface and clouds consistent with the data, though the maximum zonal wind at the cloud-top level is too strong compared to observed values. In the simulation presented here, the meridional circulation in the 65–100 km altitude region is stronger compared to the case presented in Lebonnois et al. (2010a), but the quasi-bidiurnal wave discussed in that paper is not present any more. This new simulation reproduces neatly the signature of semi-diurnal and diurnal tides above 65 km altitude. An offset in pressure, which corresponds to about 5 km in altitude, is observed in the location of the polar warming

between the model and the retrieved data presented here. The reason for this discrepancy could reflect limitations in the simulation of the aerosols distribution in the retrieval code, or to an incorrect balance between dynamics, solar heating and infrared radiative cooling in the model, possibly related to the fact that the latitudinal dependence of the cloud layer is not taken into account in the radiative module of the GCM. The uncertainty in the aerosol distribution in the retrieval code is under investigation in order to refine the accuracy of the results; however, the same method was applied to the mid-resolution data acquired by VIRTIS, and the comparison with the VeRa temperature maps (Tellmann et al., 2009) provided satisfactory results. Hence, it is unlikely to be the primary cause of the discrepancy between retrieval results and GCM model. A better representation of the cloud latitudinal distribution in the GCM is needed to improve the modelled temperature distribution.

The full longitude–latitude maps for the model temperatures (Fig. 5) at the same pressure levels as for the observations, reported in Fig. 2a–d, clearly illustrate the signatures of the semi-diurnal tide in low-latitude regions, with an increasing role of the diurnal tide for mid and high latitudes as the pressure increases.

Although not shown here, the amplitude of the diurnal component peaks in the model simulation around 60° latitude at about $5\text{--}10 \times 10^3$ Pa (around 65 and 70 km altitude), while the semi-diurnal component has one of its largest amplitude around the equator at $5\text{--}10 \times 10^2$ Pa (around 75 and 80 km altitude).

It must be noted, however, that the model provides temperatures up to 20 K higher than the retrieved values, on a global scale. On the other hand, the qualitative behaviour of the model is consistent with observations, if the shift in pressure, and hence in altitude, is taken into account. The modelled map at 32 mbar (which corresponds to about 70 km in altitude) compares quite well with the retrieved map at 100 mbar. Both are located at the level of the cold polar minimum. The maximum temperature is about 240 K, at the equator around 22 h. The cold region below 220 K is also present, at mid-to-high latitudes, showing a minimum just before 3 h in the southern hemisphere and slightly later in the northern hemisphere. The model suggests that these minima at about 60° latitude in both hemispheres correspond to the signature of the diurnal component of the thermal tide. Conversely, the maximum temperature at the equator around 22 h is created in the model by the semi-diurnal component of the thermal tide.

If only the night side (18–6 h) of the model temperature map at 32 mbar were compared to the VIRTIS-H map at 100 mbar, as well as to the corresponding southern hemisphere map in VIRTIS-M observations (Fig. 3a in Grassi et al. (2010)), one would observe a very close similarity in the locations (in latitude and local time) of minima and maxima. As already reported in the previous section, VIRTIS-H temperatures show minima at high latitudes in both hemispheres around 3 h (confirming VIRTIS-M results for the South hemisphere), and a maximum at equatorial latitudes between 22 h and 24 h. This similarity might be interpreted as the signature in VIRTIS observations of the diurnal component of the thermal tide at the latitudes of the cold collar, and of the semi-diurnal component at equatorial latitudes. If this interpretation based on the LMD Venus GCM is correct, the maximum/minimum pattern observed at the location of the cold collar would effectively correspond to a wavenumber-1 sun-synchronous wave extending into the day side and phase-shifted to locate a minimum around 3 h. The maximum at low latitudes at about 22 h would be the manifestation of a slightly phase-shifted wavenumber-2 sun-synchronous wave, similarly extending into the day side.

This interpretation is distinct from the one suggested in Grassi et al. (2010), where the maximum/minimum pattern at high latitudes was presented as the possible night side signature of the wavenumber-2 semi-diurnal component of the thermal tide. This latter interpretation is especially suggested by the comparison

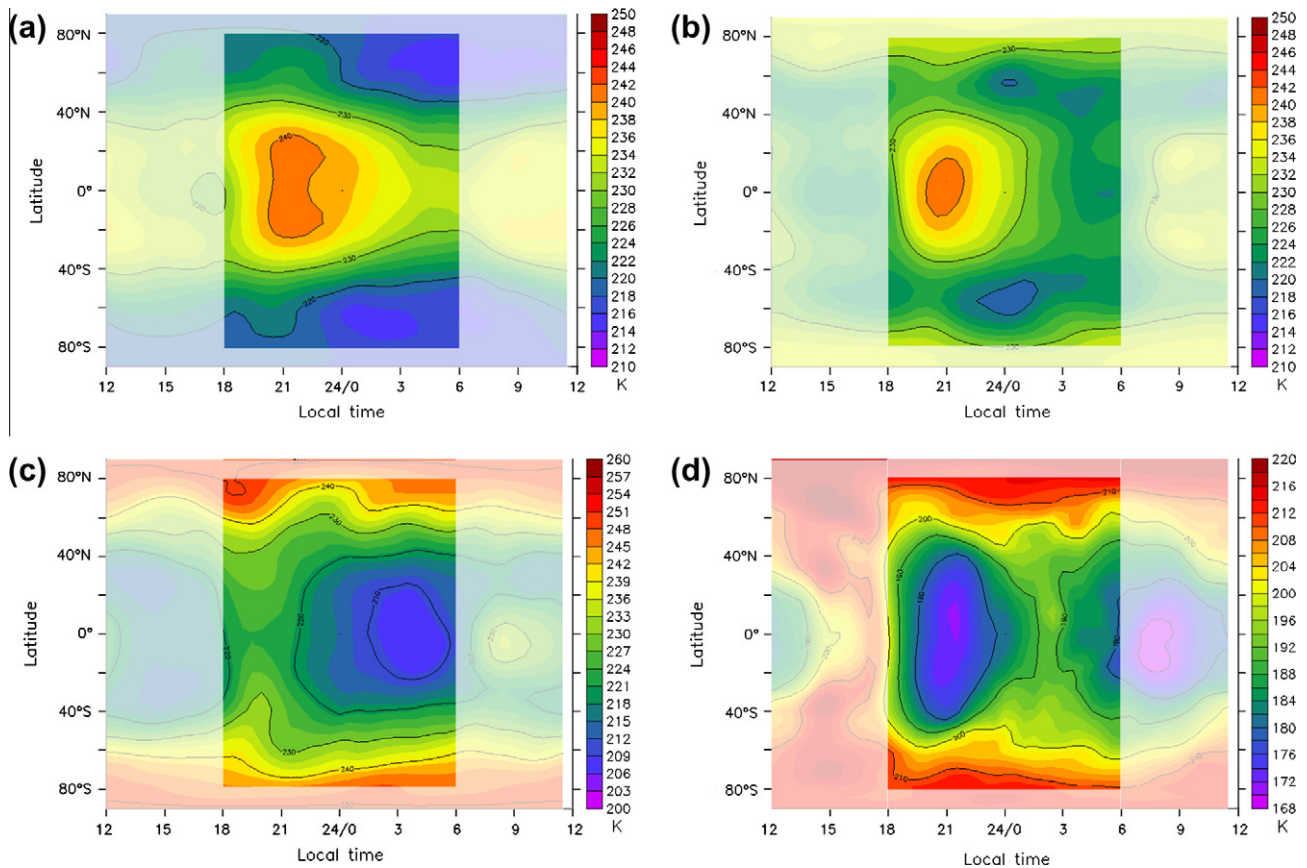


Fig. 5. Local time–latitude maps from the LMD Venus GCM simulation at (a) 32 mbar, (b) 13 mbar, (c) 4 mbar and (d) 0.5 mbar. Due to the quantitative shift in altitude of the modelled polar warming compared to observations, these levels are chosen to qualitatively correspond to the observed fields shown in Fig. 2.

with VeRa observations (Tellmann et al., 2009), where the temperature structure around 100 mbar appears to be dominated by a wave-2 solar tide with the minimum aligned with the subsolar and the antisolar points. These observations, however, are averaged between 75° and 85° latitude in both hemispheres, where the influence of the polar vortex dynamics could be significant. The minimum of temperatures in VIRTIS observations is centred more around 65° latitude. Furthermore, Elson (1983) and Zasova et al. (2002, 2007) point out that, although the wavenumber-2 seems to be dominant in most cases in OIR and FTS observations, at high latitudes between 65 and 70 km altitude (OIR) and 55–72 km altitude (FTS), the amplitude of the wavenumber-1 sun-synchronous wave exceeds that of the wavenumber-2 wave, in agreement with the LMD GCM model and the interpretation we suggest in this paper. We would like to stress that a clear attribution of the observed VIRTIS patterns of maximum/minimum temperatures at 100 mbar to the presence of diurnal and semi-diurnal components of the thermal tide can only be achieved when retrievals are available also for the NLTE-affected day side. It is not possible to draw conclusions on the longitudinal wavenumber of a signal that contains only half the longitudes, since the phases might play an important role, as Fig. 5a shows in the model. Furthermore, it is likely that the interpretation of the temperature structure at high latitudes in the venusian mesosphere is effectively a combination of diurnal and semidiurnal signals with different amplitudes, as suggested for instance by OIR observations (Schofield and Taylor, 1983).

Good agreement between observed and modelled maps is found also at other pressure levels (see Fig. 5b, c, and d for modelled maps at 13 mbar, 4 mbar and 0.5 mbar respectively). On average, the temperature trend with latitude is confirmed by the

model, as well as the local maxima at equatorial regions in the observed map at 13 mbar (see Fig. 2c).

A good correspondence between northern and southern hemispheres is also found, especially at mid-high latitudes. At lower latitudes, though the agreement between model and observations is less satisfying, temperatures still decrease from evening to morning, and the morning side tends to present local maxima for higher levels, as already found in the OIR/PV observations.

VIRTIS observations, therefore, may prove extremely important to help constrain models of Venus' atmospheric circulation.

5. Conclusions

In the present paper we extend the air temperature investigation of the Venus atmosphere, carried out for the southern hemisphere by VIRTIS-M, to the high resolution channel of VIRTIS. A valuable dataset of air temperature profiles in the altitude range between 65 and 80 km in the night side of Venus, covering most of the latitudes, was obtained. Similarities between the two hemispheres have been observed.

We report a good correspondence with the results obtained in previous investigations with VIRTIS-M and OIR, as well as evidences of wave activity. The operational extension of the Venus Express mission will allow to directly compare new data with observations acquired with OIR on Pioneer Venus at similar conditions in term of solar cycle.

Grassi et al. (2010) suggested that the pattern of temperatures at 100 mbar at around 60–65° latitude in the southern hemisphere could be the night side signature of a semi-diurnal tide, which would imply a wavenumber-2 sun-synchronous wave extending in the day side. In this paper, we showed the possible signature

of different thermal tides versus latitude in the two hemispheres. In order to suggest an interpretation for the observed patterns of average temperatures, we carried out a comparison with a global circulation model of the venusian atmosphere. Results from the LMD Venus GCM model present a very good agreement with observed air temperature maps, although the quantitative details are not fully satisfying (for instance, in the altitude and latitudinal extent of the polar warming, as well as the absolute temperature values). The agreement hints that the maximum/minimum patterns seen in the observations at 100 mbar could be signatures of the effect of diurnal and semi-diurnal tides (in particular, diurnal component at high latitudes, semi-diurnal at equatorial latitudes). Therefore, the combination of new model results obtained by Lebonnois et al. (2010b) with the inclusion of a full radiative transfer scheme, and the nearly global temperature coverage of VIRTIS-H observations suggest an interpretation for the pattern at high latitudes in terms of the diurnal component of the thermal tide, simply shifted in longitude with a minimum at about 3 h, which is different from the one included in Grassi et al. (2010).

A conclusive interpretation of these observed temperature oscillations in term of diurnal and/or semi-diurnal tidal components must be, nonetheless, postponed until a full day and night side temperatures data set will become available from VIRTIS.

The reported temperature maps are invaluable in helping to constrain the models and their predictions on the dynamics of the venusian mesosphere, such as the important role played by the tides in this region of the atmosphere in generating superrotation (see Lebonnois et al., 2010a, for a related discussion).

Acknowledgments

The authors thank ESA, ASI, CNES and the other national space agencies supporting the Venus Express mission. A. Migliorini is supported by ASI. Testing of radiative transfer tools for the Venus environment by D. Grassi was also supported by the ASI-ESS project. A special thanks is due to H. Svedhem, D. Titov and the entire ESA Venus Express staff for leading and managing such an exciting mission. These results would not have been possible without the efforts of the VIRTIS technical teams in Rome and Meudon. S. Lebonnois thanks the project Exoclimats financed by the Agence Nationale de la Recherche (ANR), and the computation facilities of both the Institut du Développement et des Ressources en Informatique Scientifique (IDRIS) and the University Pierre and Marie Curie (UPMC). The authors wish to thank Dr. Jonathan Lunine and Dr. Francesca DeMeo, for their comments which helped us to improve the English.

References

Baines, K.H. et al., 2000. Detection of sub-micron radiation from the surface of Venus by Cassini/VIMS. *Icarus* 148, 307–311.

- Bezard, B., de Bergh, C., Crisp, D., Maillard, J.P., 1990. The deep atmosphere of Venus revealed by high-resolution nightside spectra. *Nature* 345, 508–511.
- Crisp, D., Ingersoll, A.P., Hildebrand, C.E., Penston, R.A., 1990. VEGA balloon meteorological measurements. *Adv. Space Res.* 10, 109–124.
- Grassi, D. et al., 2010. Average thermal structure of venusian night-time mesosphere as observed by VIRTIS–Venus Express. *J. Geophys. Res.* 115, E09007. doi:10.1029/2009JE003553.
- Grassi, D. et al., 2008. Retrieval of air temperature profiles in the venusian mesosphere from VIRTIS-M data: Description and validation of algorithms. *J. Geophys. Res.* 113, E00B09. doi:10.1029/2008JE003075.
- Elson, L., 1983. Solar related waves in the venusian atmosphere from the cloud tops 100 km. *J. Atmos. Sci.* 40, 1535–1551.
- Lebonnois, S. et al., 2010a. Superrotation of Venus' atmosphere analysed with a full General Circulation Model. *J. Geophys. Res.* 115, E06006. doi:10.1029/2009JE003458.
- Lebonnois, S., Hourdin, F., Forget, F., Eymet, V., Fournier, R., 2010b. The LMD Venus General Circulation Model: Improvements and Questions. International Venus Conference, Aussois, 20–26 June 2010.
- Linkin, V.M. et al., 1986. Thermal structure of the Venus atmosphere in the middle cloud layer. *Science* 231, 1420–1422.
- Linkin, V.M. et al., 1987. Thermal structure of the atmosphere of Venus from the results of measurements taken by landing vehicle Vega-2. *Cosmic Res.* 25, 501–512.
- Meadow, V.S., Crisp, D., 1996. Ground-based near infrared observations of the Venus nightside: The thermal structure and water abundance near the surface. *J. Geophys. Res.* 101, 4595–4622.
- Moroz, V.I. et al., 1986. Venus spacecraft's infrared radiance spectra and some aspects of their interpretation. *Appl. Opt.* 25, 1710–1719.
- Moroz, V.I., Huntress, W.H., Shevlev, I.L., 2002. Planetary missions of the 20th century. *Kosmicheskie issledovanija* 40 (N5), 451–481 (in Russian).
- Oertel, D. et al., 1985a. Infrared experiment on VENERA-15 and VENERA-16 orbiters. Methods and first results. *Kosmicheskie issledovanija* 23, 191–205 (in Russian).
- Oertel, D. et al., 1985b. Infrared spectrometry from Venera-15 and Venera-16. *Adv. Space Res.* 5, 25–36.
- Piccioni, G. et al., in press. VIRTIS: The Visible and Thermal Imaging Spectrometer. ESA-SP 1295, ESA Publications Division, Noordwijk, The Netherlands.
- Pollack, J.B. et al., 1993. Night infrared light from Venus' night side: A spectroscopic analysis. *Icarus* 103, 1–42.
- Schofield, J.T., Taylor, F.W., 1983. Measurement of the mean solar fixed temperature and cloud structure of the middle atmosphere of Venus. *Q. J. R. Meteorol. Soc.* 109, 57–80.
- Seiff, A., 1983. Thermal structure of the atmosphere of Venus. In: Hunten, D.M., Colin, L., Donahue, T.M., Moroz, V.I. (Eds.), *Venus*. The University of Arizona Press, Tucson, Arizona, pp. 215–279.
- Seiff, A. et al., 1985. Models of the structure of the atmosphere of Venus from the surface to 100 km altitude. In: Kliore, A.J., Moroz, V.I., Keating, G.M. (Eds.), *The Venus Reference Atmosphere* (*Adv. Space Res.* 5 (11), 3–58).
- Taylor, F.W. et al., 1980. Structure and meteorology of the middle atmosphere of Venus Infrared remote sensing from the Pioneer orbiter. *J. Geophys. Res.* 85, 7963–8006.
- Taylor, F.W., Crisp, D., Bezard, B., 1997. Near infrared sounding of the lower atmosphere of Venus. In: Bougher, S.W., Hunten, D.M., Phillips, R.J. (Eds.), *Venus II*. The University of Arizona Press, Tucson, Arizona, pp. 325–352.
- Tellmann, S., Pätzold, M., Häusler, B., Bird, M.K., Tyler, G.L., 2009. Structure of the Venus neutral atmosphere as observed by the Radio Science experiment VeRa on Venus Express. *J. Geophys. Res.* 114, E00B36. doi:10.1029/2008JE003204.
- Titov, D.V. et al., 2002. Missions to Venus, Earth-like planets and moons. Proceedings of the 36th ESLAB Symposium, 3–8 June 2002.
- Titov, D.V. et al., 2006. Venus Express science planning. *Planet. Space Sci.* 54, 1279–1297.
- Zasova, L.V., Khatuntsev, I.V., Ignatiev, N.I., Moroz, V.I., 2002. Local time variations of the middle atmosphere of Venus: Solar-related structures. *Adv. Space Res.* 299, 243–248.
- Zasova, L.V., Ignatiev, N.I., Khatuntsev, I.A., Linkin, V., 2007. Structure of the Venus atmosphere. *Planet. Space Sci.* 55, 1712–1728.